ORIGINAL PAPER

CrossMark

Electrostatic Stabilization and Characterization of Fine Ground Silicon Particles in Ethanol

Markus Nöske[1] · Sandra Breitung-Faes[1] · Arno Kwade[1]

Abstract
Stirred media milling is a common method for the efficient production of nanoparticles. Here the grinding of semi-metallic silicon nanoparticles is presented, which are of special interest as anode material for next generation lithium-ion batteries. Ground silicon particles show an enormous reactivity in water due to particle etching but only surficial oxidization in alcoholic solvents, which inhibits further particle etching. Therefore, the grinding process was realized in ethanol as a solvent in order to avoid particle etching but allow good integrity to a water-based anode production later on. From the application point of view the colloidal stability of silicon nanoparticle suspensions is of great importance, to realize anode coating structures with fine disperse silicon nanoparticles. Hence, this study is focusing on the electrostatic stabilization of the silicon nanoparticles in ethanol, which was characterized by zeta potential and the agglomerate size measurements. These results corresponding to electrostatical interactions are also in good accordance with rheological characterization of the suspensions and theoretical calculations. Additionally, the final metallic silicon content was also of high interest for the application, so that a thermogravimetric analysis procedure was established and evaluated by a chemical pulping procedure according to DIN EN ISO 21068-2. Furthermore the impact of the chosen stabilization additive and the solvent purity on the silicon content are discussed. Finally the process is realized by a pre-grinding step in a planetary ball mill and a fine grinding step within a stirred media mill. With this setup a production route for suspensions with a median primary particle size of less than 150 nm and metallic silicon content above 80 wt.% of the particles is presented. The ground nanoparticles show a surficial oxidized shell with a silicon core and a flake-like shape with crystalline and amorphous regions.

1 Introduction

The application of nanoparticles with customized properties is common in a variety of industries [1–4]. The combination of nanoscale and material dependent characteristics is often the basis for innovations and enhanced product performances. Concerning this matter silicon offers several interesting opportunities. Due to its intrinsic photoluminescence which is increased by the quantum confinement effect with decreasing particle size, it is a promising candidate for the usage in opto-electronics [5, 6]. In addition, the non-toxicity of pure silicon and its degradation product (orthosilicic acid) lead to many biomedical developments such as fluorescent biomarkers [7–9], drug delivery carrier [10, 11] and silicon-based therapeutics [12]. In the semiconductor industry silicon is the main material due to its good semi- and photo-conducting properties, which can be adjusted by thermal treatment or elemental doping. The development of stable suspensions with silicon nanoparticles offers a multitude of applications in the field of printed electronics and solar cells in future [13–15]. Furthermore, theoretical ten-times higher specific capacity regarding the storage of lithium ions in an anode of a lithium-ion battery compared to graphite based anodes makes silicon a promising candidate for next generation lithium ion batteries [16–18].

In the present study the production of silicon nanoparticles in a two-step grinding procedure is established for the later

✉ Markus Nöske
m.noeske@tu-bs.de

[1]   Institute for Particle Technology, Technische Universität Braunschweig, Volkmaroder Strasse 5, 38104 Braunschweig, Germany

application in anodes of lithium ion batteries. Zhang [19] and Liu [20] showed that reversible lithiation of silicon particles can be reached with a particle size below 150 nm. Therefore, this particle size was adapted as a target size of the grinding process.

Taking into account common water-based anode processing, the mixable solvent ethanol was chosen to allow a good integrity of the silicon nanoparticles, which can be added as a ground, ethanolic silicon suspension directly to the aqueous anode suspension or previously used for the preparation of hydrophilic, silicon-based anode composites. Other advantages of this solvent are good availability and low costs for mass production in up scaled processes. Reindl et al. [21, 22] investigated the intrinsic stability and oxidation of silicon for printed electronics during dispersing in polar and non-polar solvents. They figured out that oxidation is always present in alcoholic solvents, which leads to the formation of a 1–2 nm thin oxide shell around the particles. In addition it was shown by Hou [17] that this oxide layer can have on the one hand positive effects on the battery performance regarding the cycle life of the silicon material. On the other hand a too high content of silicon oxide in the anode leads to high initial capacity losses of the battery cell due to irreversible formation of lithium silicates [16]. Thus, a range exists were fineness and silicon content of the particles are optimal for this application. In the present study the examination of the silicon oxidization in ethanol is done by Fourier-transform infrared spectroscopy, qualitatively. In addition, a thermogravimetric method is established and evaluated by a chemical pulping procedure according to DIN EN ISO 21068-2 in order to quantify the metallic silicon content of the particles. The impact of chosen formulation components on the final metallic silicon content of different suspensions with the same fineness are investigated by this method.

Ashuri, He and Shaw [16] summarized production routes for promising silicon rich anodes. They figured out that for a good anode performance the nanoscale of the silicon building blocks in combination with good introduction into a porous carbon network with high electric conductivity and mechanical flexibility are necessary. To avoid particle agglomeration and to allow good integrity of the silicon nanoparticles during mixing steps with carbon materials the colloidal stability of the particles is crucial. However, a systematic study on the stabilization of silicon nanoparticles in ethanol is missing in literature. In this study stabilization investigations are carried out by adjustment of the zeta potential and thus by increasing the repulsive particle-particle interactions, electrostatically. The latter is described by the theory of Derjaguin, Landau, Verwey, Overbeek (DLVO theory) [23] and is in good accordance to the rheological behavior of the suspension.

2 Material and Methods

2.1 Materials

As feed material for the grinding experiments silicon powder from PyroPowders GmbH, Germany, with a purity of >99.0% was used. The particle size distribution is given in Fig. 1 (analyzed by laser diffraction, sympatec Helos). The median particle size is 17 μm.

The solvents used in this study were absolute Ethanol (EtOH) from Merck KGaA, Germany, (purity 99.99%) and Ethanol technical grade (EtOH tec) from Berkel AHK Alkoholhandel GmbH, Germany (purity >96.0%). For the stabilization of the silicon particles sodium hydroxide (NaOH) from Merck KGaA, Germany, (purity 99.98%) was utilized and added as a solution of 0.5 mol NaOH in EtOH stepwise to the product suspension during the grinding experiment.

2.2 Grinding Set-up

Since the feed material was too coarse for the fine grinding procedure a pre-grinding step in a planetary ball mill PM 400 from Retsch GmbH, Germany, was performed upstream. The beads (1.5 mm) for this grinding procedure were made of tungsten carbide and obtained from Sigmund Lindner GmbH, Germany. Milling processes were performed with a filling ratio of the beads in the steel vessels (0.5 L) of 30%, a sun wheel speed of 250 rpm and a grinding time of 1 h. In each vessel 1228 g beads, 62.5 g silicon and 250 g ethanol were added successively. Thus, the ground ethanolic silicon suspensions had a solids content c_m of 20 wt.%. No additive was added during this step.

Fine grinding and stabilization investigations were performed with the stirred media mill SL-12-Nano from VMA Getzmann GmbH, Germany, which was operated in circuit mode between the mill and a stirred vessel. These experiments
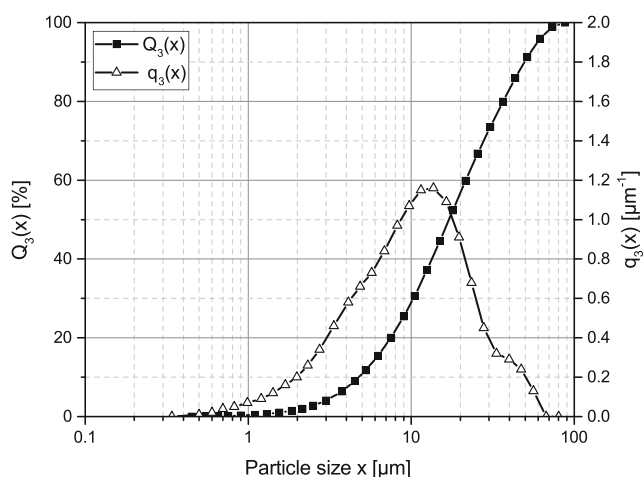

Fig. 1 Particle size distribution of silicon feed particles

were run with yttrium stabilized zirconia beads (315 μm) from Sigmund Lindner GmbH, Germany, a filling ratio of 70% and a stirrer circumferential speed of 8 m·s^{-1}. After the experiment was started with a prefilling of 300 g ethanol, 300 g of the pre-ground suspension was added to obtain a suspension with a solids content of 10 wt.%. During the experiment the pH* value was measured repeatedly and adjusted by pipetting ethanolic NaOH solution into the suspension stirred inside the circuit vessel.

The power draw P of the mill during the process time t was measured, as well as the no load power P_0 afterwards. Under consideration of the ground solids mass m the specific energy input E_m is calculated according to eq. 1.

$$E_m = \frac{\int_0^t (P(t) - P_0) \cdot dt}{m} \tag{1}$$

2.3 Analysis

2.3.1 Particle Size and Morphology

The primary particle size was analyzed by acoustic spectroscopy (acoustic) with the DT1200 of Quantachrome GmbH & Co. KG, Germany, in suspensions with original solids content. For the evaluation of the agglomerate size diluted samples using the dynamic light scattering (DLS) device Nanophox from Sympatec GmbH, Germany, was applied. The morphology of the ground product was characterized by electron microscopy with a scanning electron microscope (SEM) LEO 1550 from Carl Zeiss AG, Germany, and a transmission electron microscope (TEM) FEI Tecnai G2 F20, FEI Technologies Inc., USA. In addition, the median crystallite size of selected samples was analyzed by X-ray diffraction (XRD) using Empyrean series 2 with PIXcel-3D detector, PANalytical, Germany.

2.3.2 Particle Surface Characterization

The zeta potential ζ was investigated by measuring the colloid vibration current in the undiluted suspension with the DT1200 of Quantachrome GmbH & Co. KG, Germany. After the grinding experiments 20 ml of the suspension was centrifuged and dried carefully by vacuum evaporation at room temperature to obtain dry silicon powders. These powders were ground in mortar and analyzed by Fourier-transform infrared spectroscopy (FT-IR) using ATR Vertex V70 from Bruker AXS Inc., USA.

2.3.3 Suspension Characterization

The dynamic viscosity was characterized as a function of the shear rate by a rotational viscometer Gemini 2 from Malvern Instruments Ltd., Great Britain. In addition, the pH value analysis in ethanolic suspensions was carried out according to Barth [24] and Menon [25]. They mentioned that the pH value is originally defined for aqueous systems, but can be adapted to water-similar media like ethanol. The dissociation constant of ethanol is $10^{-19.1}$ mol^2·L^{-2} and therefore, the pH scale ranges to 19.1 [26]. For the analysis of the pH value in ethanol no specific sensor or ethanol-based calibration standards were available. Thus, the pH analysis was carried out with a standard pH electrode for aqueous systems. However, we are aware the resulting measured values are not correct from their absolute value and should only be compared to each other. The electrode WTW SenTix 41 from Xylem Analytics Germany Sales GmbH & Co. KG, Germany, was used and calibrated with aqueous standard solutions. pH values analyzed in this way were marked with pH*.

2.3.4 Quantification of Metallic Silicon Content

For the quantification of the metallic silicon content a thermogravimetric analysis (TGA) method was developed and evaluated with a chemical pulping procedure according to DIN EN ISO 21068-2 (pulping). For the development of the TGA method, nano-ground silicon samples were first treated in a TGA/DSC-Analyzer from Mettler Toledo Inc., Switzerland, for the documentation of trends during the treatment. In a second step the evaluated procedure was transferred to a procedure in a muffle furnace from Nabertherm GmbH, Germany. Details about the developed method are presented later on in section 3.3.

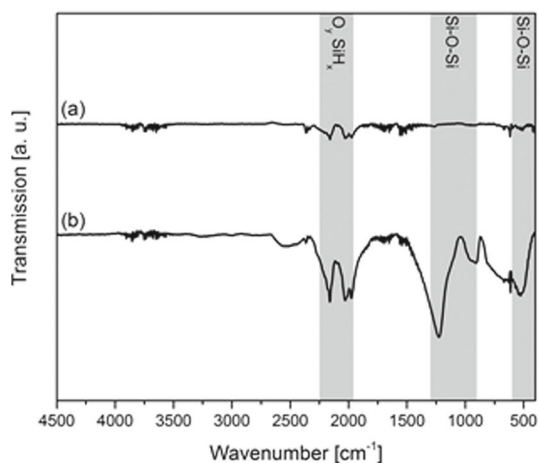## 3 Results and Discussion

3.1 Silicon Stabilization

During fine grinding of silicon in ethanol the particles tend to form agglomerates as a result of increasing ratio of attractive van der Waals forces to buoyancy and fluid forces due to the decreasing particle sizes. For aqueous systems the electrostatic stabilization of the ground particles due to the analysis and adjustment of the zeta potential ζ is a commonly known technique [27]. The latter can be adapted to ethanolic systems by manipulating the pH* value of the suspension [24]. Therefore, the dependency of both parameters was analyzed and illustrated in Fig. 2. The suspension without any additive has a pH* of 4.9 and a ζ of −15 mV after fine grinding. By increasing the pH* value to 7.5 the ζ becomes enhanced to −45 mV and is only slightly decreasing by further increase of the pH* value to 11. Based on this findings grinding experiments with three different pH* values (5, 7.5 and 10) had been carried out with equal specific energy input of 33,000 kJ·kg^{-1}. The ground suspensions exhibit only negligible deviation from the median
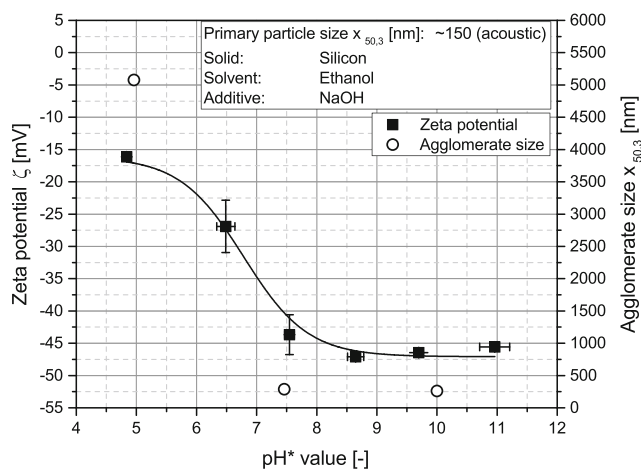
Fig. 2 Zeta potential ζ and agglomerate size dependent from the pH* value for silicon nanoparticles in ethanol

primary particle size of 150 nm, which was analyzed by acoustic spectroscopy and was set as the target size. By comparison of the median agglomerate size, measured by DLS, and the median primary particle size an indication of the colloidal stability can be obtained (Fig. 2). It becomes obvious, that at pH* 5 the particles are highly agglomerated, because a median agglomerate size of 5 μm was detected. This size can be reduced to 280 nm due to an increase of ζ at pH* 7.5 and pH* 10. Therefore, in a pH* range from 7.5 to 10 a small discrepancy of the agglomerate size from the primary particle size was found. This result can be explained by the different measurement techniques and it can be assumed that agglomeration is almost negligible.

In order to reach a better understanding with respect to the surficial reactions, which are occurring between reactive surfaces of ground silicon particles and solvent molecules, FT-IR spectra of dried samples from ground silicon and the untreated feed material were compared. The results are presented in Fig. 3. The surficial oxidation of the particles is clearly

determined due to the presence of typical adsorption bands. Si-O-Si bands are detected from 900 to 1300 cm^{-1} [28] and around 500 cm^{-1} [21, 22]. Additionally O-SiH groups are determined by several bands in a range from 2000 to 2250 cm^{-1} [28]. The reaction mechanism between silicon and alcohol was shown by Wayner et al. [29] and is also presented in Fig. 3. They outlined that this mechanism is similar to the reaction with water, but in contrast alcohols do not etch the silicon material [30]. Therefore, a thin oxide layer on the particle surface is formed, as well as hydrogen gas which has to be aspirated for safety reasons.

These experimental findings can be summarized and described with respect to colloidal stability issues more detailed with the DLVO theory [23]. The validity of this theory for ethanolic suspension systems was already shown [24, 31]. Wang et al. [31] described an pH-dependent surface charge of alumina particles in ethanol, which can be transferred for surficial oxidized silicon particles with silanol surface groups (SiOH) in basic pH environment in the following way:
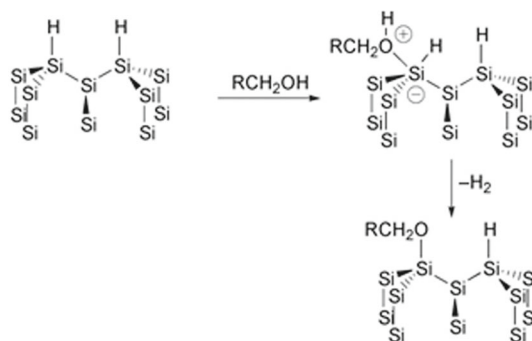
$$SiOH + OH^- \leftrightarrow SiO^- + H_2O \tag{2}$$

The total interaction potential V_{tot} of two silicon particles is the sum of the attractive van der Waals potential V_A and the repulsive electrostatic potential V_R.

$$V_{tot} = V_A + V_R \tag{3}$$

V_A between two particles of equal size can be calculated by the following equation [32]:

$$V_A = -A \cdot \frac{1}{6} \left(\frac{2}{s^2-4} + \frac{2}{s^2} + \ln \frac{s^2-4}{s^2} \right) \tag{4}$$

V_A depends on the particle radius r and the distance between the particles a. Both parameters are included in the parameter s.

Fig. 3 Left: FT-IR spectra of (**a**) feed material and (**b**) fine ground silicon particles in ethanol ($x_{50,3}$: 150 nm, acoustic) with typical IR absorption bands [21, 22, 28]; right: Reaction between alcohol and silicon [29]

$$s = \frac{(a + 2 \cdot r)}{r} \quad (5)$$

Furthermore, V_A is a material function due to the fact, that the Hamaker constant A is only dependent on material parameters of the dispersed solid A_s and the fluid A_f:

$$A = \left(\sqrt{A_s} - \sqrt{A_f} \right)^2 \quad (6)$$

For the calculation of the Hamaker constant a value of 6.3 for silica, which represents the surficial oxidized particle surface [33], and 4.2 for ethanol were used, respectively [34].

The colloidal stability of a suspension can be enhanced by an increase of the repulsive electrostatic potential V_R [24, 27, 31].

$$V_R = \frac{r}{v^2} \cdot \frac{32 \cdot \pi \cdot \varepsilon \cdot \varepsilon_0 \cdot (R \cdot T)^2}{F^2} \cdot \gamma^2 \cdot e^{-\kappa \cdot a} \quad (7)$$

The repulsive potential V_R was calculated by the particle radius r, which was half of the particle diameter $x_{50,3}$ of 150 nm. Furthermore, the dielectric coefficient of EtOH (24.35 [35]) ε, the relative permittivity ($8.85 \cdot 10^{-12}$ $C \cdot V^{-1} \cdot m^{-1}$) ε_0, the gas constant (8.314472 $J \cdot Kmol^{-1}$) R and the Faraday constant ($9.65 \cdot 10^4$ $C \cdot mol^{-1}$) F were used. A temperature T of 293.15 K was also included. The valence of the OH^- and Na^+ ions v was set equal to 1. Taken into account, that the surficial potential Ψ_0 can be replaced by ζ in good approximation [24, 31], γ was calculated by the following equation:

$$\gamma = \frac{\left(e^{\left(\frac{v \cdot F \cdot \Psi_0}{R \cdot T} \right)} - 1 \right)}{\left(e^{\left(\frac{v \cdot F \cdot \Psi_0}{R \cdot T} \right)} + 1 \right)} \quad (8)$$

The Debye parameter κ can be calculated by consideration of the ionic concentration c by:

$$\kappa = \sqrt{\frac{2 \cdot F^2 \cdot c \cdot v^2}{\varepsilon \cdot \varepsilon_0 \cdot R \cdot T}} \quad (9)$$

Furthermore, the thermic energy has to be considered for the stability of a suspension. Verwey and Overbeek [23] assumed in a first approximation a good colloidal stability for a total interaction potential V_{tot} of higher than 10 k·T. For this term the Boltzmann constant k has to be considered ($1.38064852 \cdot 10^{-23}$ $J \cdot K^{-1}$). More current investigations prove a stable colloidal system for $V_{tot} > 15$ k·T [23, 27, 32]. In order to compare V_{tot} and the thermic energy more easily, V_{tot} was normalized by dividing it by k·T. The resulting Potential curves for suspensions with three different pH* values are shown in Fig. 4 (left) as well as the corresponding rheological behavior of the suspensions (right).

The potential curve of the suspension with pH* 5 has a maximum normalized interaction potential of 5, which proves the poor colloidal stability due to the absence of a significant potential barrier against particle agglomeration. This finding correlates with a pronounced shear thinning viscosity behavior due to a high level of internal friction. It is also shown, that the colloidal stability can be effectively increased by shifting the pH* value to 7.5, which corresponds to a normalized interaction potential of almost 40 and a nearly Newtonian viscosity behavior. By further increase of the pH* value the ζ decreases only slightly (Fig. 2) but the ionic concentration c increases conversely. Therefore, the diffuse double layer close to the particles becomes less extended and as a result the potential curve is also compressed, reaching a maximum value of still more than 30. The attraction between the particles becomes higher and can be detected by a shear thinning rheological behavior of the suspension.

3.2 Silicon Grinding

Based on the stabilization investigations which show a clear optimum of increased repulsive particle-particle interaction at a pH* value of 7.5, the same stabilization was used for fine grinding tests in a stirred media mill. The results of the two-step grinding procedure are shown in Fig. 5.

The grinding results show a clear correlation of particle size reduction and increasing specific energy input. After the pre-grinding step the median particle size $x_{50,3}$ has a value of 500 nm correlating with a specific energy of 2100 $kJ \cdot kg^{-1}$. Additionally, the particle size distribution shows a wide range represented by the values of top cut $x_{90,3}$ of 1500 nm and the fines $x_{10,3}$ of 180 nm, respectively. The top cut was small enough after this step, that blocking of the flat screen, used for internal grinding media separation, during the fine grinding process could be avoided. At the end of the fine grinding process step i.e. after a specific energy input of 106,000 $kJ \cdot kg^{-1}$ the $x_{50,3}$ can be reduced further to a value of 75 nm. The particle size distribution becomes narrow shown by the $x_{90,3}$ and $x_{10,3}$ values of 190 nm and 45 nm, respectively.

In order to get impressions of the particle shape resulting from the grinding process SEM and TEM images of feed material and the ground silicon particles are shown in Fig. 6. The feed material in this study is a coarse powder with an angular particle shape (a). After a specific energy input of ~33,000 $kJ \cdot kg^{-1}$ ground silicon particles with a measured $x_{50,3}$ of ~150 nm show a flake–like particle shape (b). The diameter of a single flake plane can be attributed to the measured particle sizes in good accordance. Therefore, the particle size measured with acoustic spectroscopy can be defined as the primary particle size in this case. TEM analyses also convey the impression of a thin layered flake structure (c) with amorphous and crystalline regions (d). Hou et al. report [17] about significant amorphization of silicon particles during the

milling process, which can be seen in amorphous regions between grain boundaries. This observation can be confirmed by amorphous and crystalline regions, which are marked in Fig. 6d, inside the nanoparticle. In addition, XRD analyses show that the median crystallite size of the feed material can be reduced from 100 nm to 53 nm after the pre-grinding and further on to 10 nm after the fine grinding step. Besides it can be pointed out that in contrast to dispersing of silicon aggregates, where the particles have a spherical shape [18, 21], the thickness of the flake-like particles seem to be in the lower nanometer range.

3.3 Silicon Content Analysis

Regarding the usage of the silicon nanoparticles in anode production for lithium ion batteries Hou [17] and Tao [36] pointed out, that the amount of oxidized silicon on the one hand can lower the initial start capacity of a battery cell, while on the other hand the mechanical strength of the particles increases as well as the cycle stability of the material. During the grinding process mechanical stressing events cause the generation of fresh and unsaturated silicon surfaces after a breakage event. These surfaces are mainly saturated by oxidation reaction with solvent molecules [21] (see also Fig. 3). In order to quantify the amount of non-degraded metallic silicon content of the nanoparticles a TGA procedure was established in this work. In Fig. 7 a typical behavior of a fine ground silicon sample during the TGA procedure is shown.

The sample mass m_s was heated up under nitrogen flow in a range of 20–950 °C and held at 950 °C for 2 h. During this treatment a small mass loss m_{loss} of 2 wt.% between 20 and 200 °C, indicating organic residuals from the grinding procedure, and a high mass increase in a range of 50–60 wt.% during the holding phase at 950 °C is detected. The mass increase during the holding phase is attributed to the formation
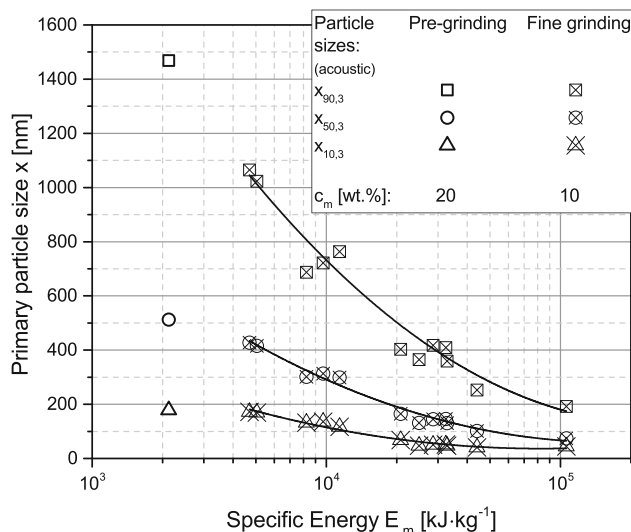

Fig. 5 Particle sizes $x_{90,3}$, $x_{50,3}$ and $x_{10,3}$ after pre-grinding and during fine grinding measured with acoustic spectroscopy and dependent on the specific energy E_m

of silicon nitride (Si_3N_4) during the melting of silicon nanoparticles, which starts at temperatures above 800 °C. This phenomena was already published by Schierning [37] and Rieke [15], who showed that the melting temperature of silicon nanoparticles is extremely reduced compared to silicon bulk material at 1410 °C. Furthermore, there were no reactions between a silicon dioxide (SiO_2) reference sample and nitrogen examined (see Fig. 7), which leads to the conclusion that any SiO_2 content in the initial sample does not taking active part on reactions during this procedure. After this sample behavior was clarified, the TGA procedure was transferred to a muffle furnace with nitrogen flushing. The mass loss m_{loss} after 200 °C and the increased mass m_{incr} after an expanded holding phase of 5 h at 950 °C were measured separately.

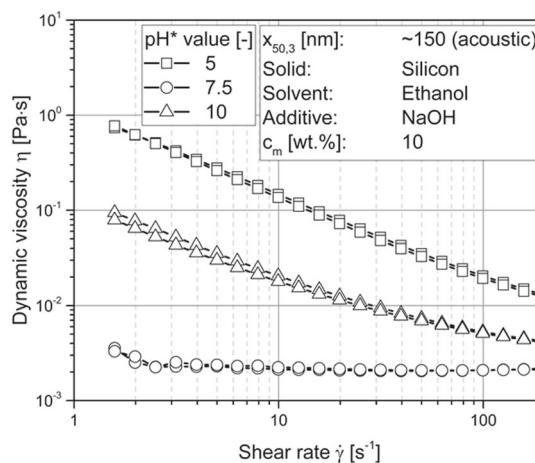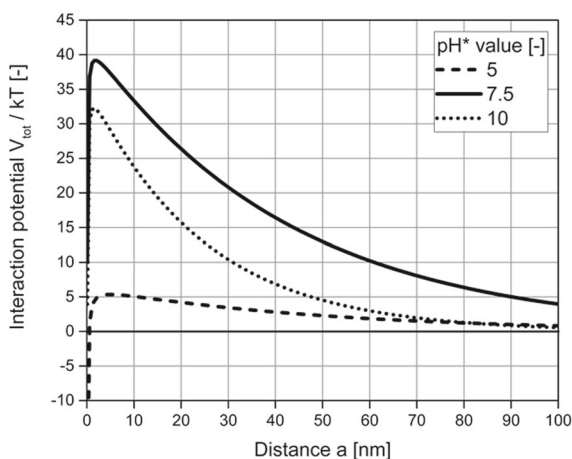For the calculation of the silicon content the inorganic sample mass $m_{s,inorg}$ was calculated.

Fig. 4 Left: Normalized interaction potential dependent on the distance from the particle surface for different pH* values; right: Dynamic viscosity as a function of shear rate for adjusted pH* values

$$m_{s,inorg} = m_s - m_{loss} \tag{10}$$

Assuming that $m_{s,inorg}$ is the mass of pure silicon and taking into account the molecular weights of silicon M_{Si} and Si_3N_4 M_{Si3N4}, the theoretical mass increase $m_{incr,theor}$ was calculated regarding a stoichiometric reaction of silicon and nitrogen.

$$3Si + 2N_2 \xrightarrow{950°C} Si_3N_4 \tag{11}$$

$$m_{incr,theor} = \left(\frac{m_{s,inorg}}{3 \cdot M_{Si}}\right) \cdot M_{Si3N4} \tag{12}$$

The increased sample mass m_{incr} analyzed by the TGA procedure was set in relation to the calculated $m_{incr,theor}$ in order to obtain finally the metallic silicon content c_{Si} of the sample.

$$c_{Si} = \frac{m_{incr}}{m_{incr,theor}} \cdot 100 \text{ wt.\%} \tag{13}$$

This value can range up to 100 wt.%. For fine ground silicon it is lowered by degradation reactions due to the presence of especially SiO_2 in the sample.
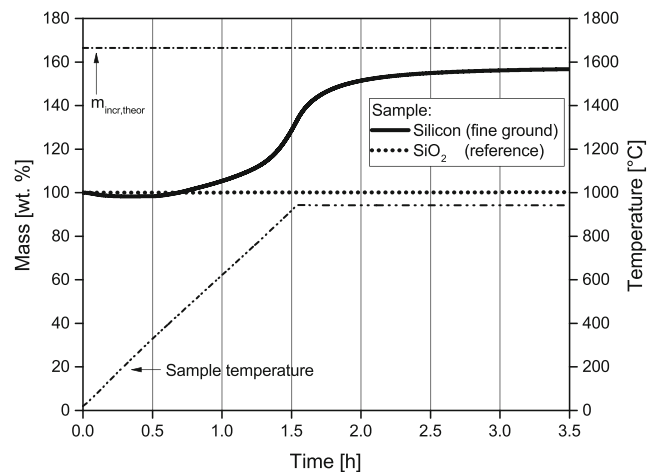

Fig. 7 Mass curve of a fine ground silicon sample during the TGA procedure in comparison to a SiO_2 reference and a calculated theoretical mass increase for the formation of Si_3N_4

In order to quantify the impact of electrostatic stabilization on the metallic silicon content c_{Si}, the pH* value was changed during the fine grinding step. After a certain specific energy
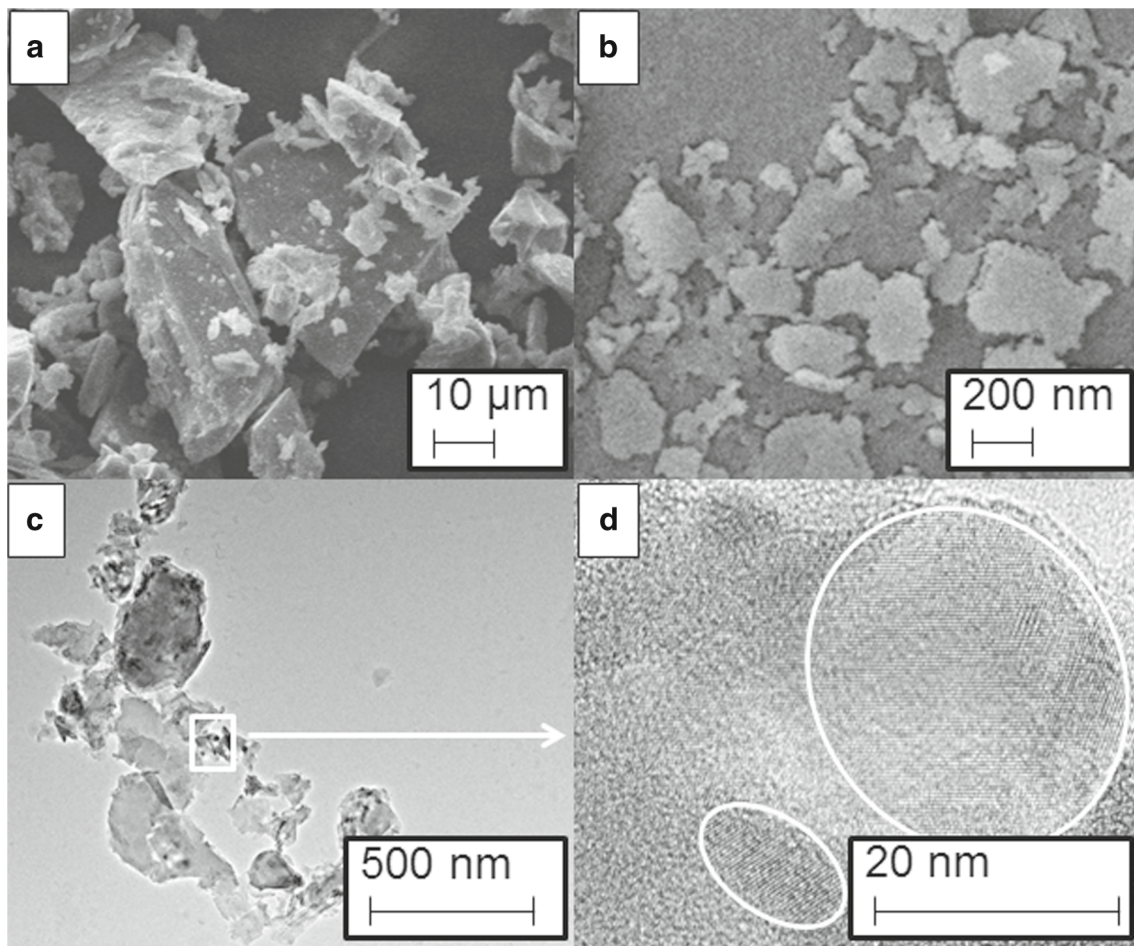
Fig. 6 SEM (**a, b**) and TEM pictures (**c, d**) of the feed material and the fine ground silicon particles: (**a**) feed material, (**b, c, d**) fine ground silicon particles ($x_{50,3}$: 150 nm, acoustic)
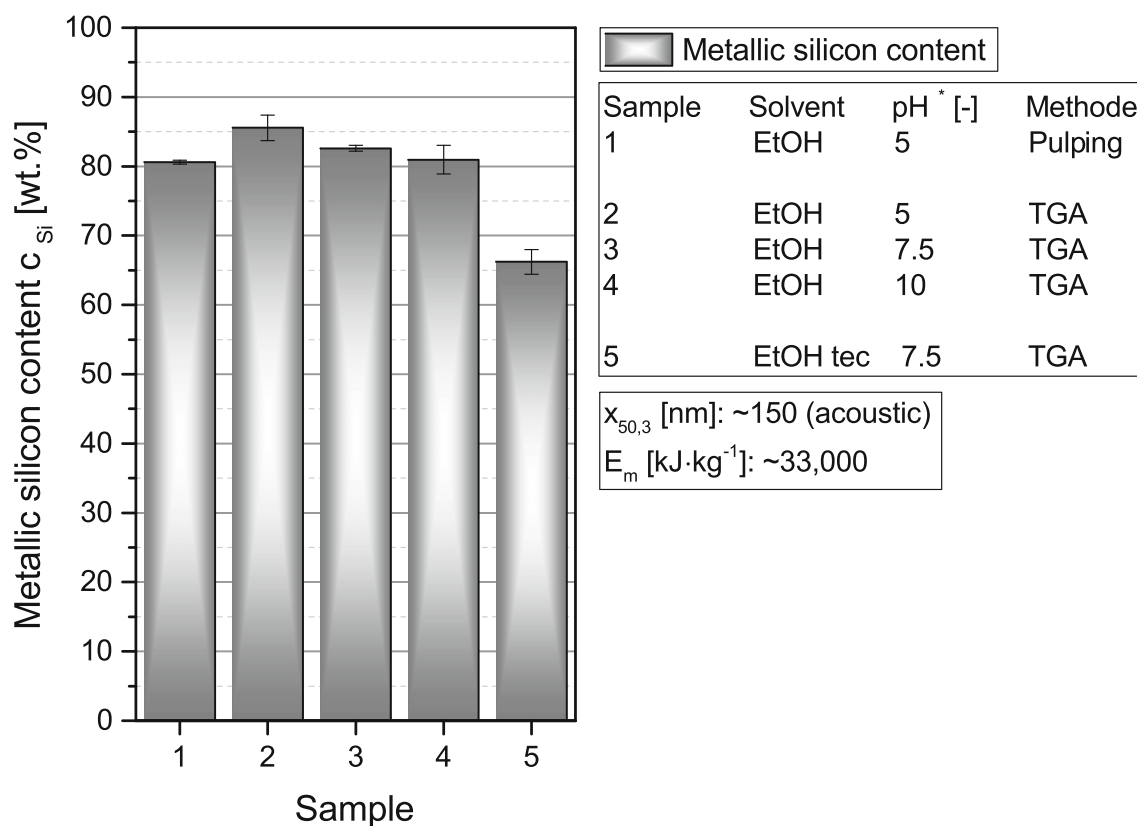
Fig. 8 Metallic silicon content c_{Si} analyzed by pulping (DIN EN ISO 21068-2) for unstabilized silicon particles at pH* 5 (1) and by a TGA: (2) at pH* 5, (3) at pH* 7.5, (4) at pH* 10 and (5) at pH* 7.5 in EtOH tec

input of 33,000 kJ·kg^{-1} a median primary particle size of 150 nm could be reached in every experiment. The metallic silicon content c_{Si} was investigated by TGA measurements directly after each experiment and evaluated with a chemical pulping method according to DIN EN ISO 21068-2 (Fig. 8). The latter one is based on an etching reaction between silicon and NaOH in boiling water, which leads to the formation of hydrogen gas. The gas volume can be measured and the silicon content can be calculated assuming a stoichiometric reaction.

Due to the addition of NaOH to the suspension, small amounts of water are formed during the reaction of NaOH and ethanol, as well as solvated Na$^+$ Ions and $C_2H_5O^-$. Especially the reaction between water and the silicon particle surface leads to increased formation of SiO_2 and lowers c_{Si} of the particles. Therefore, also the solvent quality which is mainly influenced by the water content was changed at pH* 7.5.

The samples with a pH* value of 5 analyzed by pulping and TGA show a comparable c_{Si} of 80 wt.% and 85 wt.%, respectively. At this point an uncertainty of 5 wt.% is identified, taking into account that the sample was analyzed some weeks later by pulping than by TGA. Therefore, influences regarding the storage of the suspension can't be excluded.

The addition of NaOH for pH* values of 7.5 and 10 shows only a slightly decreasing c_{Si} around 82 wt.%. Thus, the small amount of additional water results only in a marginal lowering of c_{Si}. In contrast to that the change of the solvents quality by using EtOH tec shows a major reduction of c_{Si} down to 66 wt.%. Due to the increased water content of 4 wt.% in this solvent a significant silicon oxidation occurs. The water content of the solvent is therefore a crucial parameter in order to achieve high metallic silicon content in the fine ground product.

4 Conclusions

A scaleable process route for the production of silicon nanoparticles within a two-step grinding procedure was investigated. The silicon nanoparticles show a flake-like morphology with an estimated thickness in the lower nanometer range and wide amorphous regions. At a specific energy input E_m of 33,000 kJ·kg^{-1} a median particle size $x_{50,3}$ of 150 nm and a metallic silicon content c_{Si} above 80 wt.% could be obtained.

Furthermore, electrostatic stabilization of the suspensions could be fulfilled by adding small amounts of NaOH. These investigations were carried out by measuring the pH* value,

zeta potential ζ, agglomerate size and rheological behavior of the suspensions. In addition the DLVO theory was applied for a detailed description of the stabilization mechanism. Stable suspensions were prepared by shifting the pH* value to 7.5 due to the increase of repulsive particle-particle interaction.

The material composition was characterized by FT-IR analysis and the metallic silicon content c_{Si} by a TGA procedure, which was evaluated applying a chemical pulping procedure according to DIN EN ISO 21068-2. It was shown that a surficial degradation of the silicon occurs during mechanical stressing due to oxidation reactions between reactive silicon surfaces and solvent molecules after particle breakage events. Especially the water content of the solvent influenced the extent of silicon degradation by massive lowering of the silicon content. In contrast different pH* value adjustments in a range of pH* 5 to 10 didn't result in significant differences regarding the metallic silicon content of the samples.

Further work will be done according to the scale-up of the grinding procedure by optimized formulation parameters. This will lead to a cost reduction for the production of higher amounts of silicon nanoparticles for various applications like for mass anode production of advanced lithium ion batteries. In addition, the interaction of silicon particle size, colloidal stability and oxidization could have impacts on the electrochemical anode performance.

Nomenclature a, [m], Distance; A, [J], Hamaker constant; A_f, [J], Hamaker constant fluid (ethanol); A_s, [J], Hamaker constant solid (silica); c_m, [wt.%], Solids concentration; c_{Si}, [wt.%], Metallic silicon content; E_m, [kJ·kg^{-1}], Specific Energy; F, [C·mol^{-1}], Faraday constant; m, [g], Mass; m_{incr}, [g], Mass increase; $m_{incr,theor}$, [g], Theoretical mass increase; m_{loss}, [g], Mass loss; m_s, [g], Sample mass; $m_{s,inorg}$, [g], Inorganic sample mass; M_{Si}, [g·mol^{-1}], Molecular weight of silicon; M_{Si3N4}, [g·mol^{-1}], Molecular weight of silicon nitride; P, [W], Power draw of the mill; P_0, [W], No load measurement of the mill power draw; $Q_3(x)$, [%], Particle size distribution sum weighted by volume; $q_3(x)$, [µm^{-1}], Particle size density distribution weighted by volume; r, [m], Particle radius; R, [J Kmol^{-1}], Gas constant; T, [°C], Temperature; t, [s], time; V_A, [J], Attractive van der Vaals potential; V_R, [J], Repulsive electrostatic potential; V_{tot}, [J], Total interaction potential; x, [nm] [µm], Particle size; $x_{50,3}$, [nm], Volume based median particle size; γ̇, [s^{-1}], shear rate; ε, [−], Dielectric coefficient; $ε_0$, [C·V^{-1}·m^{-1}], Electric constant; ζ, [mV], Zeta potential; η, [Pa·s], Dynamic viscosity; κ, [m^{-3}], Debye parameter; ν, [−], Valence; $Ψ_0$, [V], Surface potential

References

1. Barth N, Zimmermann M, Becker AE, Graumann T, Garnweitner G, Kwade A (2015) Influence of TiO2 nanoparticle synthesis on the properties of thin coatings. Thin Solid Films 574:20–27. https://doi.org/10.1016/j.tsf.2014.11.038
2. Steiner D, Finke JH, Kwade A (2018) Instant ODFs - development of an intermediate, nanoparticle-based product platform for individualized medication. Eur J Pharm Biopharm 126:149–158. https://doi.org/10.1016/j.ejpb.2017.04.014
3. Hesselbach J, Barth N, Lippe K, Schilde C, Kwade A (2015) Process chain and characterisation of nanoparticle enhanced composite coatings. Adv Powder Technol 26(6):1624–1632. https://doi.org/10.1016/j.apt.2015.09.006
4. Jux M, Finke B, Mahrholz T, Sinapius M, Kwade A, Schilde C (2017) Effects of Al(OH)O nanoparticle agglomerate size in epoxy resin on tension, bending, and fracture properties. J Nanopart Res 19(4):241. https://doi.org/10.1007/s11051-017-3831-9
5. Pillai S, Catchpole KR, Trupke T, Zhang G, Zhao J, Green MA (2006) Enhanced emission from Si-based light-emitting diodes using surface plasmons. Appl Phys Lett 88(16):161102. https://doi.org/10.1063/1.2195695
6. Boyraz O, Jalali B (2005) Demonstration of directly modulated silicon Raman laser. Opt Express 13(3):796. https://doi.org/10.1364/OPEX.13.000796
7. Wang L, Reipa V, Blasic J (2004) Silicon nanoparticles as a luminescent label to DNA. Bioconjug Chem 15(2):409–412. https://doi.org/10.1021/bc030047k
8. Tasciotti E, Liu X, Bhavane R, Plant K, Leonard AD, Price BK, Cheng MMC, Decuzzi P, Tour JM, Robertson F, Ferrari M (2008) Mesoporous silicon particles as a multistage delivery system for imaging and therapeutic applications. Nat Nanotechnol 3(3):151–157. https://doi.org/10.1038/nnano.2008.34
9. Park J-H, Gu L, von MG et al (2009) Biodegradable luminescent porous silicon nanoparticles for in vivo applications. Nat Mater 8(4):331–336. https://doi.org/10.1038/nmat2398
10. Bimbo LM, Mäkilä E, Laaksonen T, Lehto VP, Salonen J, Hirvonen J, Santos HA (2011) Drug permeation across intestinal epithelial cells using porous silicon nanoparticles. Biomaterials 32(10):2625–2633. https://doi.org/10.1016/j.biomaterials.2010.12.011
11. Näkki S, Rytkönen J, Nissinen T, Florea C, Riikonen J, Ek P, Zhang H, Santos HA, Närvänen A, Xu W, Lehto VP (2015) Improved stability and biocompatibility of nanostructured silicon drug carrier for intravenous administration. Acta Biomater 13:207–215. https://doi.org/10.1016/j.actbio.2014.11.019
12. Zhang K, Loong SLE, Connor S et al (2005) Complete tumor response following intratumoral 32P BioSilicon on human hepatocellular and pancreatic carcinoma xenografts in nude mice. Clin Cancer Res 11(20):7532–7537. https://doi.org/10.1158/1078-0432.CCR-05-0400
13. Drahi E, Blayac S, Saunier S, Valdivieso F, Bartholin MC, Grosseau P, Benaben P (2011) Recovering functional properties of solution processed silicon thin-films. Energy Procedia 10:144–148. https://doi.org/10.1016/j.egypro.2011.10.167

14. Drahi E, Gupta A, Blayac S, Saunier S, Benaben P (2014) Characterization of sintered inkjet-printed silicon nanoparticle thin films for thermoelectric devices. Phys Status Solidi A 211(6):1301–1307. https://doi.org/10.1002/pssa.201300180

15. Riecke A (2017) Thermische Umwandlung dünner Silizium-Schichten. Friedrich-Alexander-Universität Erlangen-Nürnberg, Dissertation

16. Ashuri M, He Q, Shaw LL (2016) Silicon as a potential anode material for Li-ion batteries: where size, geometry and structure matter. Nanoscale 8(1):74–103. https://doi.org/10.1039/c5nr05116a

17. Hou X, Zhang M, Wang J, Hu S, Liu X, Shao Z (2015) High yield and low-cost ball milling synthesis of nano-flake Si@SiO2 with small crystalline grains and abundant grain boundaries as a superior anode for Li-ion batteries. J Alloys Compd 639:27–35. https://doi.org/10.1016/j.jallcom.2015.03.127

18. Li F-S, Wu Y-S, Chou J, Wu NL (2015) A dimensionally stable and fast-discharging graphite-silicon composite Li-ion battery anode enabled by electrostatically self-assembled multifunctional polymer-blend coating. Chem Commun (Camb) 51(40):8429–8431. https://doi.org/10.1039/c4cc09825k

19. X-y Z, Song W-L, Liu Z et al (2017) Geometric design of micron-sized crystalline silicon anodes through in situ observation of deformation and fracture behaviors. J Mater Chem A 5(25):12793–12802. https://doi.org/10.1039/C7TA02527K

20. Liu XH, Zhong L, Huang S, Mao SX, Zhu T, Huang JY (2012) Size-dependent fracture of silicon nanoparticles during lithiation. ACS Nano 6(2):1522–1531. https://doi.org/10.1021/nn204476h

21. Reindl A, Aldabergenova S, Altin E, Frank G, Peukert W (2007) Dispersing silicon nanoparticles in a stirred media mill - investigating the evolution of morphology, structure and oxide formation. Phys Stat Sol (A) 204(7):2329–2338. https://doi.org/10.1002/pssa.200622557

22. Reindl A, Voronov A, Gorle PK, Rauscher M, Roosen A, Peukert W (2008) Dispersing and stabilizing silicon nanoparticles in a low-epsilon medium. Colloids Surf A Physicochem Eng Asp 320(1–3):183–188. https://doi.org/10.1016/j.colsurfa.2008.01.045

23. Verwey EJW, Overbeek JZG (1948) Theory of the stability of lyophobic colloids: the interaction of sol particles having an electric double layer. Elsevier Publishing Company, New York - Amsterdam - London - Brussels

24. Barth N, Schilde C, Kwade A (2014) Influence of electrostatic particle interactions on the properties of particulate coatings of titanium dioxide. J Colloid Interface Sci 420:80–87. https://doi.org/10.1016/j.jcis.2014.01.005

25. Menon M, Decourcelle S, Ramousse S, Larsen PH (2006) Stabilization of ethanol-based alumina suspensions. J American Ceramic Society 89(2):457–464. https://doi.org/10.1111/j.1551-2916.2005.00744.x

26. Mussini T, Covington AK, Longhi P, Rondinini S (1985) Criteria for standardization of pH measurements in organic solvents and water + organic solvent mixtures of moderate to high permittivities. Pure Appl Chem 57(6):865–876. https://doi.org/10.1351/pac198557060865

27. Müller RH, Mehnert W, Paulke B-R (1996) Zetapotential und Partikelladung in der Laborpraxis. Einführung in die Theorie, Praktische Meßdurchführung, Dateninterpretation. Wissenschaftliche Verlagsgesellschaft mbH Stuttgart, Stuttgart

28. Riikonen J, Salomäki M, van Wonderen J, Kemell M, Xu W, Korhonen O, Ritala M, MacMillan F, Salonen J, Lehto VP (2012) Surface chemistry, reactivity and pore structure of porous silicon oxidized by various methods. Langmuir 28(28):10573–10583. https://doi.org/10.1021/la301642w

29. Wayner DDM, Wolkow RA (2002) Organic modification of hydrogen terminated silicon surfaces1. J Chem Soc Perkin Trans 2(1):23–34. https://doi.org/10.1039/b100704l

30. Newton TA, Huang Y-C, Lepak LA, Hines MA (1999) The site-specific reactivity of isopropanol in aqueous silicon etching: controlling morphology with surface chemistry. J Chem Phys 111(20):9125–9128. https://doi.org/10.1063/1.479386

31. Wang G, Sarkar P, Nicholson PS (1996) Influence of acidity on the electrostatic stability of alumina suspensions in ethanol. J Am Ceram Soc

32. Lagaly G, Schulz O, Zimehl R (1997) Dispersionen und Emulsionen: Eine Einführung in die Kolloidik feinverteilter Stoffe einschließlich der Tonminerale. Steinkopff, Heidelberg

33. Reindl A, Peukert W (2008) Intrinsically stable dispersions of silicon nanoparticles. J Colloid Interface Sci 325(1):173–178. https://doi.org/10.1016/j.jcis.2008.05.042

34. Israelachvili JN (2015) Van der Waals forces between particles and surfaces. In: Israelachvili JN (ed) Intermolecular and surface forces3rd edn. Elsevier Science, Saint Louis, pp 253–289

35. Schmidt VM (2003) Elektrochemische Verfahrenstechnik. WILEY-VCH, Weinheim

36. Tao H-C, Yang X-L, Zhang L-L, Ni SB (2014) Double-walled core-shell structured Si@SiO2@C nanocomposite as anode for lithium-ion batteries. Ionics 20(11):1547–1552. https://doi.org/10.1007/s11581-014-1138-8

37. Schierning G, Theissmann R, Wiggers H, Sudfeld D, Ebbers A, Franke D, Witusiewicz VT, Apel M (2008) Microcrystalline silicon formation by silicon nanoparticles. J Appl Phys 103(8):84305. https://doi.org/10.1063/1.2903908